TECHNICAL ARTICLE

Tetrapotassium pyrophosphates γ- and δ-K$_4$P$_2$O$_7$

Armel Le Bail,[1,a)] Thomas Hansen,[2] and Wilson A. Crichton[3]

[1]*Institut des Molécules et des Matériaux du Mans, CNRS UMR 6283, Université du Maine, Avenue O. Messiaen, 72085 Le Mans, France*
[2]*Institut Laue Langevin, 38042 Grenoble, France*
[3]*European Synchrotron Radiation Facility, BP 220, 38043 Grenoble, France*

The structures of γ- and δ-K$_4$P$_2$O$_7$ are solved by X-ray powder diffraction (conventional laboratory X-ray and synchrotron data, respectively), both in hexagonal symmetry ($a_\gamma = 5.9645(3)$ Å, $c_\gamma = 14.4972(8)$ Å, $V_\gamma = 446.64(4)$ Å^3 at 300 °C, $Z_\gamma = 2$, space group $P6_3/mmc$; $a_\delta = 10.211\,45(7)$ Å, $c_\delta = 42.6958(4)$ Å, $V_\delta = 3855.59(7)$ Å^3 at room temperature, $Z_\delta = 18$, space group $P6_1$) with cell–supercell relations $a_\delta \approx a_\gamma\sqrt{3}$ and $c_\delta \approx 3\,c_\gamma$. In the experimental conditions, the expected β/γ transition previously announced at 486 °C is not observed; the γ-form is stable at least up to the maximum temperature of our measurements (700 °C). In the γ-form, similar to the orthorhombic form of Na$_4$P$_2$O$_7$, idealized, the pyrophosphate group is in eclipsed conformation, the K$^+$ cations occupying three different coordinations. In the $\delta\delta$-form, two of the three different [P$_2$O$_7$]$^{4-}$ groups are staggered and one eclipsed, the K$^+$ cations occupying 12 independent sites. © *2013 International Centre for Diffraction Data*. [doi:10.1017/S0885715612000954]

Key words: tetrapotassium pyrophosphate, powder diffraction, crystal structure, *ab initio*

I. INTRODUCTION

Tetrapotassium pyrophosphate (TKPP) K$_4$P$_2$O$_7$ is a material widely used as a sequestrant, dispersant and deflocculant. It is found in daily-life chemical formulations as an industrial or household detergent builder, tooth cleaning agent, and ingredient in the food industry (E450v). It is applied to cyanide-free electroplating, can be used as a stabilizer for hydrogen peroxide, or as dispersion agent for ceramic, clay, latex, and pigments. It is employed frequently as a component in solid or liquid fertilizers (60% solubility in water). Despite the millions of tons of commercialized TKPP, none of the four anhydrous forms have been characterized crystallographically, though the polymorphic transitions were examined by thermal, X-ray, and dilatometric methods (α/β transition at 1080 °C, β/γ at 486 °C, and γ/δ at 280 °C) by Znamierowska (1978). The room temperature δ-form is highly hygroscopic, leading rapidly to K$_4$P$_2$O$_7$•3H$_2$O when exposed to air, so that most industrial users without care are probably dealing with the trihydrate. The structure of this hydrated form was determined from single crystal data (Dumas and Galigné, 1974). TKPP also repeatedly appears during investigations of a huge list of phase diagrams including the important Ln$_2$O$_3$–K$_2$O–P$_2$O$_5$ oxide systems (Szczygieł *et al.*, 2010 and references therein), though the existence of the β-form was contested (Sandström, 2006). Indeed, only two anhydrous forms were long believed to exist (Durif, 1995) before the Znamierowska work, and a complete series of solid solutions was defined in the Na$_4$P$_2$O$_7$–K$_4$P$_2$O$_7$ system (Morey *et al.*, 1955). Finally, Shekhtman *et al.* (2000) concluded that there were three polymorph modifications of K$_4$P$_2$O$_7$ below 300 °

C, denoted γ above 290 °C, but α below 270 °C and claimed a β-form in the 270–290 °C range, never citing Znamierowska's previous work. Staying in the Znamierowska notation, the existence and crystal structures of the β-, γ-, and δ-K$_4$P$_2$O$_7$ forms, are the subject of the present paper. The high temperature α-form with the α/β transition at 1080 °C very close to the fusion at 1105 °C (Znamierowska, 1978) was not accessible with our X-ray instrumentation. In spite of the absence of single crystals, solving the structures is realized from powder diffraction data by using methodologies which have demonstrated their efficiency during repeated blind tests (Le Bail *et al.*, 2009).

II. EXPERIMENTAL

The thermal behaviour of a K$_4$P$_2$O$_7$ sample from Sigma–Aldrich was followed by temperature resolved powder diffractometry (TXRD) (Siemens D5000 θ/θ diffractometer equipped with an Elphyse position-sensitive detector and a HTK10 Anton Paar temperature attachment). The sample was dusted on a platinum foil serving as heating source in a chamber pumped under vacuum, then filled with dried helium. A light He flow was maintained during the experiment. The time interval between successive powder patterns was 2880 s, including a measuring time of 2580 s; the temperature was increased by steps of 10 °C starting from 30 to 700 °C. Cu$K\alpha$ radiation was used; measurements were from 9° to 139° in 0.03°2θ steps. A contour scale plot is shown in Figure 1. The starting material contained traces of the hydrated phase which retransformed readily at 50 °C into the δ-K$_4$P$_2$O$_7$ anhydrous phase. The expected $\delta \to \gamma$ transition occurs at ~280 °C; however, the event announced at 486 °C for the $\gamma \to \beta$ transition (Znamierowska, 1978) remains undetected up to 700 °C, confirming the similar non-observation (by thermal analysis and
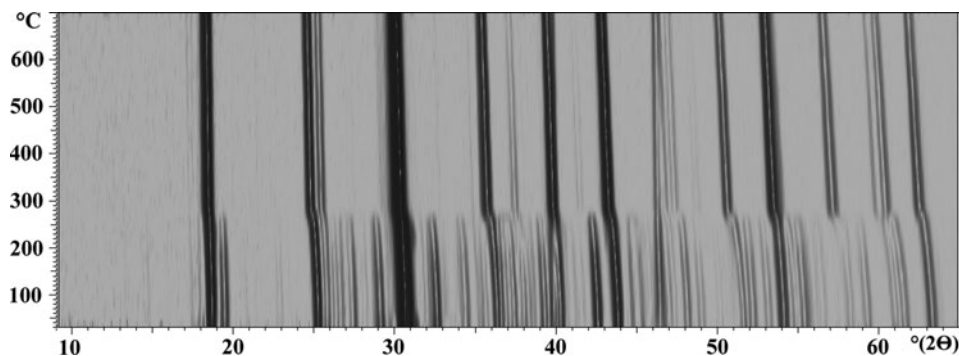
Figure 1.   TXRD contour plot (Cu$K\alpha$).
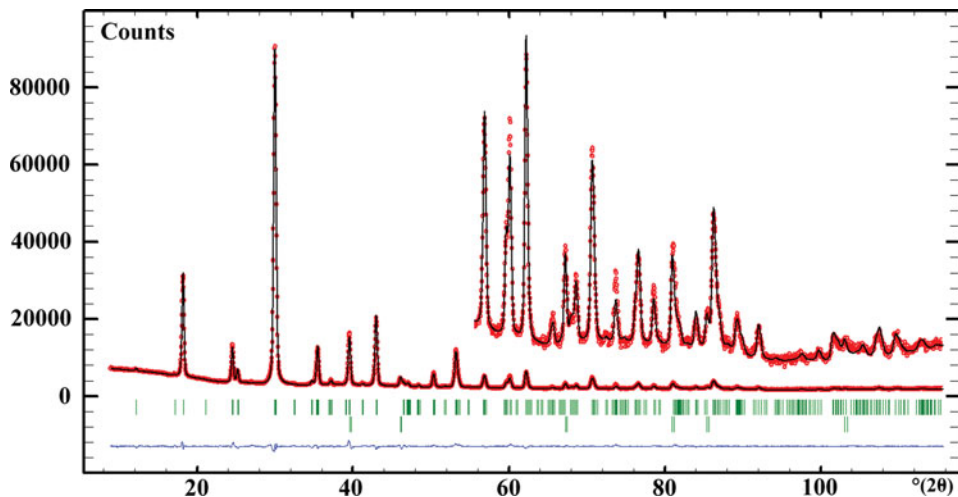
Figure 2.   Rietveld plot for γ-K$_4$P$_2$O$_7$ at 300 °C (Cu$K\alpha$). The second phase corresponds to the Pt holder.
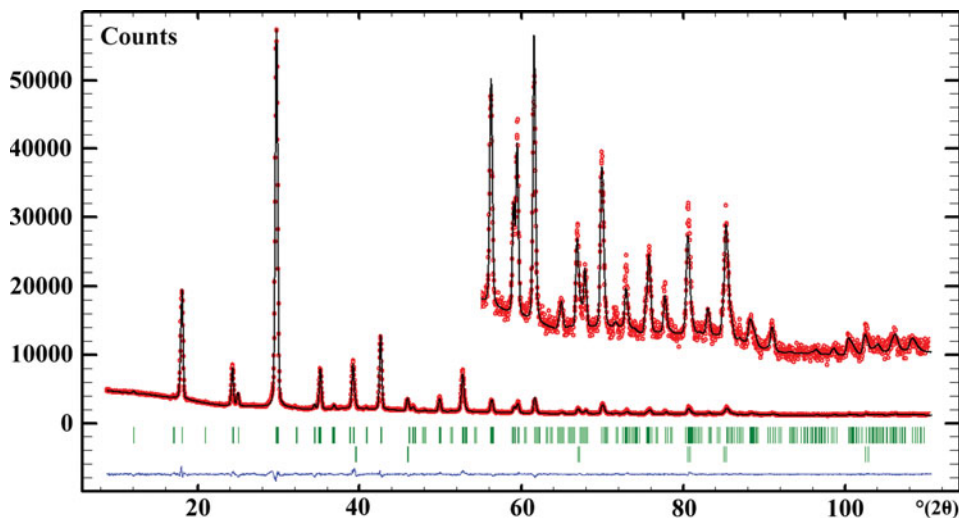
Figure 3.   Rietveld plot for K$_4$P$_2$O$_7$ at 600 °C (Cu$K\alpha$). The second phase corresponds to the Pt holder.

powder TXRD by 100 °C steps, no indexing) by Sandström (2006). Another TXRD was performed in the range 30–300–30 °C in steps of 5 °C in the 260–300–260 °C range and 10 °C elsewhere, establishing the reversibility of the transition which, under these conditions, appears to be close to 275 °C, also showing pre-transitional effects (accelerated cell parameter and intensities changes) occurring in the 230–270 °C range. Events in the 220–250 °C range during fast (3 °C/min) neutron thermodiffractomy experiments (instrument D20, ILL, Grenoble) confirmed the possibility of another phase transition close to 270 °C by Shekhtman *et al.* (2000), but these data were of no help in indexing attempts (see the neutron contour plots in

Diffractometer		Siemens D5000
Geometry		Bragg-Brentano
Goniometer		horizontal
Radiation type		Cu$K\alpha$
Wavelengths (Å)		1.540 56, 1.544 33
Position sensitive detector		Elphyse
Pattern refinement range (°2θ)		9–115
Step size (2θ)		0.03
Chemical formula		$K_4P_2O_7$
Space group		$P6_3/mmc$
Z		2
Temperature (°C)	300	600
Cell parameter (Å)		
a	5.9645(3)	6.0117(3)
c	14.4972(8)	14.6215(9)
Volume (Å^3)	446.64(4)	457.64(4)
COD number (Gražulis et al., 2009)	30 00 011	30 00 012
No. of contributing reflections		215
No. of refined parameters (total)		55
No. of atomic coordinates parameters		4
No. of restraints		None
No. of isotropic thermal parameters		6
No. of background parameters		39
(interpolated from a set of points)		
Profile shape		Pseudo-Voigt
η	0.488(6)	0.377(7)
U	0.11(1)	0.23(2)
V	0.000(2)	−0.18(2)
W	0.084(2)	0.114(3)
Conventional Rietveld reliability factors		(Rietveld, 1969)
R_P (%)	8.43	11.5
R_{WP} (%)	7.55	9.05
R_{exp} (%)	3.90	5.24
R_B (%)	3.19	3.21
R_F (%)	4.81	5.89

supplementary material available at http://journals.cambridge.org/pdj)). Given the difficulties in solving the δ-$K_4P_2O_7$ crystal structure from such conventional laboratory or neutron data (due to the large cell dimensions), a synchrotron pattern was recorded at ESRF (Grenoble) on the ID31 instrument (Fitch, 2004), $\lambda = 0.399\ 90$ Å from a sample loaded in a (0.9 mm) capillary as trihydrate, dried and fired at 500 °C, then sealed in the oven.

	Wyckoff	x	y	z	U_{iso}	BV
Kl	4f	1/3	2/3	0.5897(1)	0.052(1)	0.66
				0.5911(2)	0.069(1)	0.61
K2	2b	0	0	1/4	0.041(2)	1.03
					0.054(3)	0.91
K3	2a	0	0	1/2	0.041(2)	1.54
					0.066(3)	1.41
P	4f	1/3	2/3	0.3558(2)	0.0264(8)	5.34
				0.3548(2)	0.035(1)	5.40
O1	12k	0.1945(3)	2x	0.3826(2)	0.0660(9)	2.02
		0.1968(4)		0.3833(2)	0.091(1)	1.98
O2	2c	1/3	2/3	1/4	0.080(3)	2.42
					0.107(4)	2.43

P–O1	3x	1.486 (2)	K1–O1	6x	3.023 (2)
		1.481 (2)			3.046 (3)
P–O2		1.533 (2)	K1–O1	3x	3.327 (3)
		1.532 (3)			3.355 (4)
P–P		3.066 (3)	K2–O1	6x	2.781 (2)
		3.065 (4)			2.828 (3)
P–K1		3.392 (3)	K3–O1	6x	2.633 (2)
		3.456 (4)			2.667 (2)

III. INDEXING, STRUCTURE DETERMINATIONS AND RIETVELD REFINEMENTS

A. γ-$K_4P_2O_7$ at 300 and 600 °C from conventional X-ray data

The γ-form being simpler than the one at room temperature, it was first indexed easily in a hexagonal cell by various software, including *McMaille* (Le Bail, 2004). The FoMs (Figures of Merit) for the pattern selected at 300 °C were $M_{20} = 54.6$ (de Wolf, 1968), $F_{20} = 54.5$ (0.0111, 33) (Smith and Snyder, 1979) and $McM_{20} = 165.5$ (Le Bail, 2008). The cell volume suggested $Z = 2$. Using Le Bail fitting (Le Bail, 2005) for evaluating the reliability of the indexing and for intensity extraction, the $P6_3/mmc$ space group was the most probable. The structure solution was carried out in direct space using the *ESPOIR* software (Le Bail, 2001), moving in the cell (by a Monte Carlo process) various numbers of K, P, and O atoms. This led to the best solution with $R = 14\%$ on the first 120 *hkl* extracted at low diffraction angles. Refinements were undertaken by Rietveld (1969) *FULLPROF* software (Rodriguez-Carvajal, 1993). Patterns in the 280–700 °C range could be fitted continuously with the structural model of the γ-form. No clear-cut event was observed on the cell parameters or atomic coordinates as a function of temperature. This confirms the same non-observation of the β/γ phase transition at 486 °C by Sandström (2006). This transition thermal effect was described by Znamierowska (1978) appearing only "as a result of prolonged heating of powdered melts at 500 °C and is rather weak." The Rietveld fits for the λ-form at 300 °C and at 600 °C (much above the expected β/γ transition at 486 °C) are shown in Figures 2 and 3. The 115–139°2θ range was excluded from the refinement, being essentially dominated by two peaks from the Pt holder. The Rietveld refinement details, the atomic coordinates, selected geometric parameters, and X-ray diffraction data are shown in Tables I–IV, respectively.

B. δ-$K_4P_2O_7$ from synchrotron data

The room-temperature phase could not be indexed from low-resolution TXRD data. A large hexagonal cell could be deduced from new conventional data (Cu$K\alpha$) from a Rigaku Miniflex diffractometer (an oven-dried sample was transferred to the standard flat-plate holder and stored in a heat-sealed plastic bag 'immediately'), but the structure solution was not obtained until synchrotron data (ESRF – Grenoble, instrument ID31, $\lambda = 0.399\ 90$ Å) were recorded. Various indexing software including McMaille, yielded a hexagonal supercell with $a_\delta = a_\gamma\sqrt{3}$ and $c_\delta = 3\ c_\gamma$, leading to $Z = 18$ ($M_{20} = 84.3$, $F_{20} = 749$ (0.0005, 43) and $McM_{20} = 181.4$). Since the only

$2\theta_{obs}$	d_{obs}	I_{obs}	h	k	l	$2\theta_{cal}$	d_{cal}	I_{cal}	$\Delta 2\theta$
12.190	7.2547	0.4	0	0	2	12.200	7.2486	0.6	−0.002
17.106	5.1793	0.5	1	0	0	17.152	5.1654	0.1	−0.046
18.191	4.8727	29.6	1	0	1	18.217	4.8658	25.0	−0.026
21.115	4.2041	0.2	1	0	2	21.102	4.2066	0.1	0.013
24.538	3.6248	11.2	0	0	4	24.542	3.6243	8.6	−0.004
25.210	3.5297	3.4	1	0	3	25.216	3.5289	2.9	−0.006
29.980	2.9781	100.0	1	1	0	29.937	2.9822	58.7	0.043
			1	0	4	30.096	2.9668	41.3	−0.116
32.324	2.7673	0.4	1	1	2	32.436	2.7580	0.1	−0.112
34.736	2.5804	0.9	2	0	0	34.705	2.5827	1.2	0.031
35.448	2.5302	11.1	2	0	1	35.269	2.5427	1.0	0.179
			1	0	5	35.475	2.5283	9.9	−0.027
37.159	2.4175	1.6	0	0	6	37.181	2.4162	1.1	−0.022
39.499	2.2796	15.6	2	0	3	39.531	2.2778	11.5	−0.032
41.204	2.1891	0.6	1	0	6	41.214	2.1886	0.5	−0.010
42.956	2.1038	20.7	2	0	4	42.966	2.1033	19.3	−0.010
46.442	1.9536	1.5	2	1	0	46.475	1.9523	1.0	−0.033
47.029	1.9306	1.2	2	1	1	46.919	1.9349	0.5	0.110
			2	0	5	47.083	1.9285	0.6	−0.054
48.441	1.8776	0.6	1	1	6	48.447	1.8774	0.6	−0.006
50.321	1.8118	4.4	0	0	8	50.310	1.8121	2.2	0.011
			2	1	3	50.368	1.8102	1.8	−0.047
51.762	1.7647	0.2	2	0	6	51.769	1.7644	0.3	−0.007
53.179	1.7209	11.8	3	0	0	53.150	1.7218	6.2	0.029
			2	1	4	53.249	1.7188	5.0	−0.070
56.811	1.6192	3.7	2	1	5	56.803	1.6194	2.3	0.008
			2	0	7	56.946	1.6157	1.7	−0.135
59.652	1.5487	2.0	1	1	8	59.654	1.5487	1.8	−0.002
60.112	1.5380	3.9	1	0	9	60.120	1.5378	3.2	−0.008
62.195	1.4914	5.3	2	2	0	62.206	1.4911	5.7	−0.011
65.609	1.4218	0.5	3	1	1	65.407	1.4257	0.2	0.202
			2	1	7	65.669	1.4206	0.3	−0.060
68.597	1.3669	1.3	2	0	9	68.608	1.3668	1.1	−0.011
70.663	1.3220	3.6	3	1	4	70.641	1.3323	3.2	0.022
73.667	1.2849	1.2	3	1	5	73.700	1.2844	0.9	−0.033
76.571	1.2432	1.7	2	1	9	76.625	1.2425	1.8	−0.054
78.567	1.2166	1.1	4	0	4	78.577	1.2164	1.0	−0.010

systematic extinction corresponds to 00l, $l = 6n$, the space group is either $P6_122$, $P6_522$, $P6_1$ or $P6_5$. Incomplete starting models were obtained either by the direct method approach using SHELXS (Sheldrick, 2008) or in direct space by using ESPOIR (Le Bail, 2001). However, given the clear relation between both phases, refinements were attempted by starting

directly from the γ-K$_4$P$_2$O$_7$ structure expanded, using the CRYSCON software (Dowty, 2006), to fit in all possible space groups for the supercell, and using restraints forcing the existence of the P$_2$O$_7$ groups. A best fit was clearly obtained in the $P6_1$ space group. Anisotropic line broadening was detected and treated phenomenologically by separating the
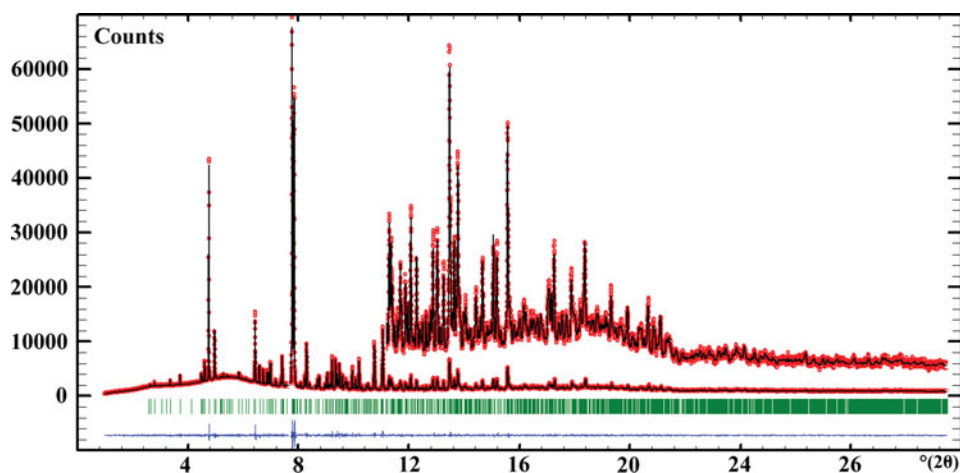

Figure 4. Rietveld plot for δ-K$_4$P$_2$O$_7$ (synchrotron powder pattern on instrument ID31, ESRF) at room temperature ($\lambda = 0.399\,90$ Å).

Diffractometer	Beamline ID31 (ESRF)
Geometry	Debye-Scherrer
Radiation (synchrotron)	0.399 90 Å
Sample holder	Capillary
Pattern range (°2θ)	1–31.5
Step size (2θ)	0.002°
Chemical formula	$K_4P_2O_7$
Space group	$P6_1$
Z	18
Cell parameter (Å)	
$\quad a$	10.211 45 (7)
$\quad c$	42.6958 (4)
Volume (Å^3)	3855.59 (7)
COD number (Gražulis et al., 2009)	30 00 010
No. of contributing reflections	3407
No. of refined parameters (total)	185
No. of atomic coordinates parameters	116
No. of restraints	60
No. of isotropic thermal parameters	3
No. of background parameters	47
(interpolated from a set of points)	
Profile shape	Pseudo-Voigt
η	0.459(6)
U	0.0812(6)
V	0
W	0.000 030(2)
Conventional Rietveld reliability factors	(Rietveld, 1969)
R_P (%)	9.25
R_{WP} (%)	8.71
R_{exp} (%)	5.85
R_B (%)	3.25
R_F (%)	2.05

peaks into three categories, $00l$, $hk0$, and the others, obtaining a decrease from $R_P = 12.8\%$ and $R_{WP} = 13.7\%$ to $R_P = 9.25\%$ and $R_{WP} = 8.71\%$. The $hk0$ lines present the smallest full width at half maximum (0.0055–0.0680°) in the whole °2θ range (2–31°) and the $00l$ lines present the largest ones (0.0191–0.0924°); other lines show FWHMs between 0.0083° and 0.0805°. The Rietveld fit is in Figure 4, the Rietveld refinement details, the atomic coordinates, selected geometric parameters, and X-ray diffraction data are shown in Tables V–VIII, respectively.

IV. STRUCTURES DESCRIPTIONS AND DISCUSSION

The γ-form (Figure 5) looks like an idealized view of the structure of $Na_4P_2O_7$, which, though orthorhombic (space group $P2_12_12_1$), is pseudo-hexagonal with $a \sim b\sqrt{3}$ and with a similar c parameter (Leung and Calvo, 1972). The distorted 6-fold coordinations of two of the four independent Na sites disposed in chains of cations along the c-axis in $Na_4P_2O_7$ become K3 and K2 alternating octahedra and trigonal prisms (TPs) sharing faces (Figure 6). The two other Na sites in the tetrasodium pyrophosphate in 5-fold coordination become K1 in a strange 9-fold coordination with a hexagonal face as a basis of the polyhedron and a triangle from a PO_4 tetrahedron face at the top. Two such polyhedra have their hexagonal face building an empty hexagonal prism of oxygen atoms (Figure 7). The pyrophosphate group is in an eclipsed conformation. Two potassium-rare-earth silicates $K_3RESi_2O_7$ ($RE = $ Lu, Sc) adopt a similar structure as γ-$K_4P_2O_7$, same space group and very close cell parameters, the rare-earth replacing the K3 atom in octahedral coordination (Vidican et al., 2003; Napper et al.,

TABLE VI. Fractional atomic coordinates and isotropic displacement parameters (Å^2) for the δ-$K_4P_2O_7$ form in the $P6_1$ space group (all atoms in general Wyckoff position 6a); $\Delta\gamma$ is the amplitude of the displacement (Å) of the atoms after joining their sites in the γ-form at 300 °C; BV is the bond-valence calculated according to Brese and O'Keefe (1991).

Atom	x	y	z	U_{iso}	$\Delta\gamma$	BV
K1	0.3041(6)	0.3892(6)	0.27646(14)	0.0210(3)	0.78	1.09
K2	0.2946(6)	−0.0075(6)	0.20455(12)	0.0210(3)	0.76	0.94
K3	0.9995(6)	1.0366(6)	0.16267(16)	0.0210(3)	0.41	1.02
K4	1.0029(6)	0.0354(5)	0.24872(14)	0.0210(3)	0.35	1.24
K5	0.3466(5)	0.2755(6)	0.60834(13)	0.0210(3)	0.70	1.19
K6	0.3490(5)	0.3219(5)	0.95177(12)	0.0210(3)	0.33	1.14
K7	0.2775(6)	0.9274(6)	0.55312(13)	0.0210(3)	0.67	0.89
K8	0.4159(6)	0.0535(7)	0.88773(14)	0.0210(3)	0.74	0.96
K9	0.3021(6)	0.6853(5)	0.16560(17)	0.0210(3)	0.45	1.14
K10	0.6580(8)	0.3767(5)	0.16655(19)	0.0210(3)	0.49	1.45
K11	0.3179(5)	0.7326(7)	0.25110(13)	0.0210(3)	0.77	1.16
K12	0.5891(6)	0.3221(6)	0.25000*	0.0210(3)	0.74	1.00
P1	0.2841(3)	0.3720(3)	0.19718(5)	0.0066(4)	0.80	4.84
P2	0.2753(3)	−0.0434(2)	0.36569(5)	0.0066(4)	0.55	4.82
P3	0.2933(3)	0.0211(3)	0.29666(5)	0.0066(4)	0.55	4.84
P4	0.3723(3)	0.3950(3)	0.13060(5)	0.0066(4)	0.55	4.81
P5	0.3857(3)	0.3518(3)	0.86794(6)	0.0066(4)	0.47	4.84
P6	0.3608(3)	0.3125(3)	0.79736(6)	0.0066(4)	0.43	4.84
O1	0.2744(7)	0.2390(5)	0.21457(13)	0.0114(5)	0.73	1.85
O2	0.2592(8)	−0.1846(5)	0.38081(14)	0.0114(5)	0.68	2.07
O3	0.3526(7)	0.5168(5)	0.21557(13)	0.0114(5)	0.44	1.93
O4	0.4218(4)	0.0963(5)	0.37430(15)	0.0114(5)	0.50	2.03
O5	0.1353(4)	0.3340(7)	0.18222(14)	0.0114(5)	0.44	1.87
O6	0.1387(5)	−0.0261(8)	0.37097(16)	0.0114(5)	0.57	2.05

Continued

Table VI. Continued

Atom	x	y	z	U_{iso}	$\Delta\gamma$	BV
O7	0.4347(5)	0.0474(7)	0.28001(14)	0.0114(5)	0.90	1.92
O8	0.3475(7)	0.5246(5)	0.12215(16)	0.0114(5)	0.48	2.06
O9	0.3035(8)	0.1674(4)	0.30690(15)	0.0114(5)	0.82	1.81
O10	0.2382(5)	0.2433(4)	0.12278(15)	0.0114(5)	0.48	1.99
O11	0.1502(5)	−0.0781(6)	0.27867(14)	0.0114(5)	0.82	2.00
O12	0.5182(5)	0.4144(7)	0.11709(14)	0.0114(5)	0.75	2.13
O13	0.4000(4)	0.4037(5)	0.16820(5)	0.0114(5)	0.70	2.08
O14	0.2826(6)	−0.0711(4)	0.32845(4)	0.0114(5)	0.68	2.08
O15	0.2819(6)	0.2315(5)	0.89075(11)	0.0114(5)	0.96	2.00
O16	0.3841(7)	0.4983(4)	0.87082(15)	0.0114(5)	0.53	2.10
O17	0.5434(4)	0.3747(7)	0.86810(16)	0.0114(5)	0.75	2.10
O18	0.3826(7)	0.4662(4)	0.78944(15)	0.0114(5)	0.64	1.97
O19	0.2268(5)	0.1855(5)	0.78077(13)	0.0114(5)	0.52	2.14
O20	0.5029(5)	0.3034(8)	0.79406(16)	0.0114(5)	0.57	2.03
O21	0.3128(4)	0.2838(5)	0.83399(4)	0.0114(5)	0.44	2.05

*Fixed origin along the z-axis.

2004). For the γ-form, the P–O distances were not constrained, resulting in values reasonably close to the standard ones (Table III), though the bond valence calculated values (Table II) are far too large for K3 (1.54 instead of 1) in 6-fold coordination and too small for K1 (0.66). This, and the fact that the P–O distances are slightly shorter at 600 °C than at 300 °C, gives another proof that the accuracy from powder data cannot beat that from a single crystal. For the δ-form, in spite of the synchrotron data quality, strong divergences occurred with the expected values so that the P–O distances were restrained to be close to those in the $CaK_2P_2O_7$ crystal structure (Sandström *et al.*, 2003), with the P–O bond involved in the P–O–P at 1.634 Å and the others at 1.514 Å. The δ-form projections along the c-axis (Figure 8) and along the [110]-direction (Figure 9) evidence helicoïdal (6_1) modulation of the pyrophosphate groups and of the K⁺ cations, with considerable moves (though always less than 1 Å, see the amplitude $\Delta\gamma$ of the displacement for each atom Table VI) if compared with the γ-form (Figure 5). However, such displacements are larger than those occurring at the phase transition, since the intensities and positions of the diffraction peaks of the δ-form continuously evolve closer to those of the γ-form in the range 20–260 °C. Unfortunately, a refinement at 260° from the conventional X-ray laboratory data is even more unstable than from the synchrotron data at room temperature and the atomic coordinates would be too uncertain. The coordinations of the K atoms (with upper limitation to K–O = 3.5 Å) are no longer as symmetrical as they were in the γ-form. We examine first those K1, K2, K5, K6, K7, and K8 atoms which will become the K1 type in the γ-form (coordination 6 + 3). In no case does the hexagonal plane of six oxygen atoms exist at room temperature; it transforms each time into a distorted plane of 5 oxygen atoms. Moreover, the PO₄ tetrahedron face providing three oxygen atoms is sometimes

TABLE VII.   Selected interatomic distances (Å) for the δ-$K_4P_2O_7$ form.

K1–O	K2–O	K3–O	K4–O	K5–O	K6–O
O1 2.994(8)	O1 2.661(9)	O1 3.356(8)	O1 2.893(7)	O2 2.816(9)	O5 2.971(8)
O3 2.838(8)	O4 2.844(6)	O5 2.762(8)	O6 2.694(10)	O4 3.298(9)	O7 2.604(6)
O9 2.609(9)	O6 2.836(7)	O6 2.631(10)	O10 2.736(8)	O6 3.452(8)	O8 2.842(10)
O10 2.790(7)	O7 3.455(8)	O9 3.161(11)	O11 2.643(9)	O8 2.810(7)	O10 2.859(6)
O12 2.951(10)	O9 3.041(8)	O10 2.855(7)	O15 2.688(9)	O11 2.540(8)	O15 2.734(7)
O18 2.828(8)	O11 3.413(8)	O11 3.237(9)	O19 2.678(6)	O12 2.775(8)	O19 2.793(7)
O20 2.849(8)	O16 2.822(10)	O19 2.822(9)		O18 2.847(10)	O20 2.952(10)
	O17 2.930(6)	O21 2.862(8)		O19 2.813(7)	
K7–O	**K8–O**	**K9–O**	**K10–O**	**K11–O**	**K12–O**
O2 2.944(7)	O2 2.906(9)	O3 2.944(9)	O2 2.669(9)	O3 2.840(10)	O1 3.257(9)
O3 2.699(11)	O4 2.820(10)	O4 2.724(9)	O12 2.682(10)	O4 2.752(8)	O2 2.806(6)
O6 2.983(10)	O5 2.667(7)	O5 3.188(8)	O13 2.784(10)	O7 3.073(9)	O7 2.752(7)
O15 2.942(7)	O8 3.129(9)	O7 3.219(9)	O14 2.767(6)	O11 3.371(10)	O8 2.810(9)
O16 2.835(6)	O10 3.317(9)	O8 2.666(10)	O17 2.476(10)	O12 2.594(7)	O17 2.733(9)
O18 3.468(8)	O12 3.118(9)	O9 2.983(10)	O20 2.634(11)	O16 2.655(8)	O18 2.640(8)
O19 2.840(8)	O15 2.771(11)	O13 3.486(9)		O20 2.742(9)	
O20 3.485(9)	O17 2.981(9)	O16 2.623(8)			
		O18 2.988(7)			
P1–O	**P2–O**	**P3–O**	**P4–O**	**P5–O**	**P6–O**
O1 1.507(7)	O2 1.512(6)	O7 1.508(6)	O8 1.510(8)	O15 1.510(5)	O18 1.509(6)
O3 1.503(5)	O4 1.508(4)	O9 1.509(6)	O10 1.505(4)	O16 1.509(6)	O19 1.510(5)
O5 1.509(6)	O6 1.508(8)	O11 1.507(5)	O12 1.515(7)	O17 1.507(6)	O20 1.506(8)
O13 1.629(4)	O14 1.623(3)	O14 1.624(4)	O13 1.625(3)	O21 1.619(3)	O21 1.621(3)

TABLE VIII.   X-ray diffraction data for the δ-K$_4$P$_2$O$_7$ form ($\lambda = 0.399\ 90$ Å). Observed values from EVA software (Bruker).

$2\theta_{obs}$	d_{obs}	I_{obs}	h	k	l	$2\theta_{cal}$	d_{cal}	I_{cal}	$\Delta 2\theta$
2.591	8.8446	0.2	0	1	0	2.591	8.8434	0.1	0.000
2.647	8.6580	0.5	0	1	1	2.646	8.6596	0.2	0.001
2.806	8.1651	1.0	0	1	2	2.805	8.1701	0.6	0.001
3.053	7.5068	0.3	0	1	3	3.051	7.5114	0.2	0.002
3.220	7.1162	0.2	0	0	6	3.220	7.1160	0.2	0.000
3.365	6.8107	1.3	0	1	4	3.365	6.8098	0.8	0.000
3.732	6.1413	2.3	0	1	5	3.731	6.1428	1.7	0.001
4.489	5.1052	1.9	1	1	0	4.489	5.1057	1.1	0.000
4.521	5.0693	1.9	1	1	1	4.521	5.0696	1.3	0.000
4.617	4.9643	5.4	1	1	2	4.615	4.9657	3.7	0.002
4.769	4.8054	58.5	1	1	3	4.769	4.8058	41.6	0.000
4.978	4.6045	12.8	1	1	4	4.976	4.6059	10.1	0.002
5.015	4.5700	0.9	0	1	8	5.016	4.5693	0.8	−0.001
5.186	4.4194	0.5	0	2	0	5.184	4.4217	0.3	0.002
5.229	4.3830	0.5	1	1	5	5.230	4.3821	0.3	−0.001
5.294	4.3298	0.9	0	2	2	5.294	4.3298	0.8	0.000
5.429	4.2221	0.5	0	2	3	5.428	4.3298	0.6	0.001
5.857	3.9137	1.4	1	1	7	5.855	3.9151	1.4	0.002
5.964	3.8433	0.5	0	1	10	5.962	3.8449	0.3	0.002
6.105	3.7551	0.4	0	2	6	6.104	3.7557	0.5	0.001
6.445	3.5569	19.8	0	0	12	6.443	3.5580	18.1	0.002
			0	1	11	6.450	3.5542	1.2	−0.005
6.598	3.4747	4.6	1	1	9	6.597	3.4754	5.3	0.001
6.735	3.4041	3.9	0	2	8	6.733	3.4049	3.9	0.002
6.856	3.3437	0.9	1	2	0	6.859	3.3425	0.6/0.1	−0.003
			2	1	0				
6.881	3.3318	3.8	1	2	1	6.880	3.3323	1.1/2.0	0.001
			2	1	1				
6.943	3.3022	3.9	1	2	2	6.943	3.3022	1.4/1.7	0.000
			2	1	2				
7.001	3.2746	6.3	1	1	10	7.000	3.2753	7.1	0.001
7.189	3.1894	1.8	1	2	4	7.188	3.1897	1.3/0.4	0.001
			2	1	4				
7.367	3.1122	1.7	1	2	5	7.366	3.1125	1.2/0.4	0.001
			2	1	5				
7.422	3.0893	8.4	1	1	11	7.420	3.0899	10.4	0.002
7.464	3.0717	1.0	0	2	10	7.465	3.0714	1.0	−0.001
7.579	3.0253	0.8	1	2	6	7.579	3.0253	0.2/0.6	0.000
			2	1	6				
7.780	2.9475	100.0	0	3	0	7.779	2.9478	83.8	0.001
7.794	2.9419	73.2	0	3	1	7.797	2.9408	53.6	−0.003
7.858	2.9182	84.1	1	1	12	7.855	2.9191	100.0	0.003
8.074	2.8401	0.7	0	3	4	8.070	2.8414	0.7	0.004
8.096	2.8324	1.2	1	2	8	8.095	2.8328	0.9/0.6	0.001
			2	1	8				
8.231	2.7862	3.1	0	3	5	8.230	2.7864	3.4	0.001
8.305	2.7613	12.5	1	1	13	8.302	2.7622	17.5	0.003
8.395	2.7317	1.4	1	2	9	8.393	2.7324	0.3/1.2	0.002
			2	1	9				
8.420	2.7238	0.9	0	3	6	8.421	2.7234	1.1	−0.001
8.644	2.6531	0.7	0	3	7	8.641	2.6541	0.9	0.003
8.716	2.6315	2.5	1	2	10	8.714	2.6319	2.8/0.4	0.002
			2	1	10				
8.762	2.6175	3.5	1	1	14	8.760	2.6182	4.8	0.002
8.981	2.5538	1.3	0	1	16	8.978	2.5547	1.7	0.003
9.057	2.5326	4.2	1	2	11	9.056	2.5328	1.1/4.5	0.001
			2	1	11				
9.132	2.5117	1.4	2	2	3	9.128	2.5128	0.7	0.004
			0	2	14	9.134	2.5105	1.4	−0.002
9.231	2.4848	9.0	1	1	15	9.226	2.4861	12.2	0.005
9.354	2.4523	8.2	1	3	0	9.352	2.4527	7.4/0.7	0.002
			3	1	0				
9.414	2.4366	5.0	1	3	2	9.414	2.4366	1.4/2.9	0.000
			3	1	2				
			1	2	12	9.416	2.4361	1.2/0.1	−0.002
			2	1	12				

Continued

Table VIII. Continued

$2\theta_{obs}$	d_{obs}	I_{obs}	h	k	l	$2\theta_{cal}$	d_{cal}	I_{cal}	$\Delta 2\theta$
9.493	2.4163	6.8	1	3	3	9.490	2.4171	0.7/3.2	0.003
			3	1	3				
			0	1	17	9.495	2.4160	6.2	−0.002
9.547	2.4027	0.8	2	2	6	9.546	2.4029	1.1	0.001
9.596	2.3905	3.9	1	3	4	9.596	2.3905	0.7/3.8	0.000
			3	1	4				
9.679	2.3700	1.6	0	0	18	9.671	2.3720	1.8	0.008
9.705	2.3637	2.1	1	1	16	9.700	2.3650	3.1	0.005
9.732	2.3572	2.7	1	3	5	9.731	2.3574	2.3/0.4	0.001
			3	1	5				
9.794	2.3422	1.9	1	2	13	9.793	2.3426	1.9/0.9	0.001
			2	1	13				
9.893	2.3188	0.5	1	3	6	9.893	2.3188	0.4/0.1	0.000
			3	1	6				
9.963	2.3027	6.0	2	2	8	9.962	2.3030	7.4	0.001
10.047	2.2836	0.4	0	2	16	10.042	2.2847	0.6	0.005
10.082	2.2755	3.1	1	3	7	10.082	2.2756	2.9/1.3	0.000
			3	1	7				
10.206	2.2480	8.5	2	2	9	10.206	2.2480	10.8	0.000
10.297	2.2282	1.1	1	3	8	10.295	2.2286	0.7/0.9	0.002
			3	1	8				
10.472	2.1911	1.1	2	2	10	10.472	2.1911	1.5	0.000
10.532	2.1785	1.5	1	3	9	10.531	2.1787	0.1/1.8	0.001
			3	1	9				
			0	1	19	10.535	2.1787	0.7	−0.003
10.670	2.1505	0.4	1	1	18	10.667	2.1512	0.7	0.003
10.759	2.1327	13.5	2	2	11	10.758	2.1329	19.0	0.001
11.065	2.0739	17.7	2	2	12	11.064	2.0742	24.8	0.001
11.236	2.0426	0.7	0	4	8	11.236	2.0426	1.3	0.000
11.321	2.0272	3.5	2	3	0	11.312	2.0288	1.7/0.4	0.009
			3	2	0				
			2	3	1	11.325	2.0265	0.1/3.2	−0.004
			3	2	1				
11.387	2.0155	3.0	2	2	13	11.386	2.0156	4.1	0.001
11.427	2.0084	2.0	2	3	3	11.427	2.0084	1.2/0.9	0.000
			3	2	3				
11.515	1.9931	0.9	2	3	4	11.515	1.9931	1.0/0.1	0.000
			3	2	4				
11.627	1.9740	1.1	2	3	5	11.628	1.9739	0.2/1.1	−0.001
			3	2	5				
11.727	1.9573	2.3	2	2	14	11.725	1.9575	3.7	0.002
11.764	1.9511	1.5	2	3	6	11.764	1.9511	1.3/0.7	0.000
			3	2	6				
11.905	1.9280	1.9	1	4	1	11.907	1.9278	1.4/0.6	−0.002
			4	1	1				
11.940	1.9225	1.0	1	4	2	11.943	1.9219	0.2 / 0.6	−0.003
			4	1	2				
12.008	1.9115	1.1	0	3	17	12.007	1.9117	1.4	0.001
12.104	1.8965	3.9	2	3	8	12.105	1.8964	2.2/3.1	−0.001
			3	2	8				
12.195	1.8823	0.3	1	4	5	12.196	1.8823	0.3/0.3	−0.001
			4	1	5				
12.308	1.8652	2.5	2	3	9	12.307	1.8654	3.1/0.5	0.001
			3	2	9				
12.357	1.8578	0.6	1	3	15	12.355	1.8580	0.4/0.8	0.002
			3	1	15				
12.529	1.8324	0.9	2	3	10	12.529	1.8324	0.1/1.2	0.000
			3	2	10				
12.651	1.8148	1.1	1	4	8	12.651	1.8148	0.9/0.4	0.000
			4	1	8				
12.770	1.7980	0.8	2	3	11	12.770	1.7980	0.7/0.4	0.000
			3	2	11				
12.913	1.7781	3.2	0	0	24	12.907	1.7790	5.9	0.006
13.058	1.7585	3.3	1	4	10	13.058	1.7585	2.6/2.3	0.000
			4	1	10				
13.088	1.7545	1.6	1	3	17	13.086	1.7547	1.2/0.7	0.002

Continued

Table VIII. Continued

$2\theta_{obs}$	d_{obs}	I_{obs}	h	k	l	$2\theta_{cal}$	d_{cal}	I_{cal}	$\Delta 2\theta$
			3	1	17				
13.289	1.7280	2.4	1	4	11	13.289	1.7280	1.8/2.0	0.000
			4	1	11				
13.504	1.7007	8.3	3	3	1	13.505	1.7006	10.6	−0.001
13.534	1.6969	3.9	3	3	2	13.537	1.6965	1.3	−0.003
			1	4	12	13.539	1.6963	2.0/2.0	−0.005
			4	1	12				
13.677	1.6792	2.8	1	1	24	13.671	1.6799	3.6	0.006
13.804	1.6638	5.2	1	4	13	13.804	1.6638	4.7/4.6	0.000
			4	1	13				
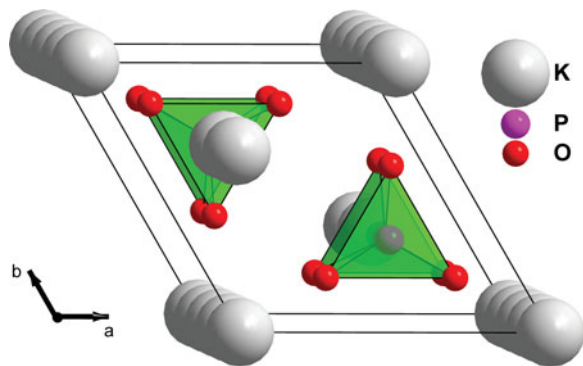
Figure 5. Projection along the *c*-axis of the structure of γ-$K_4P_2O_7$ at 300 °C showing the eclipsed pyrophosphate groups, and columns of potassium atoms K2 and K3.
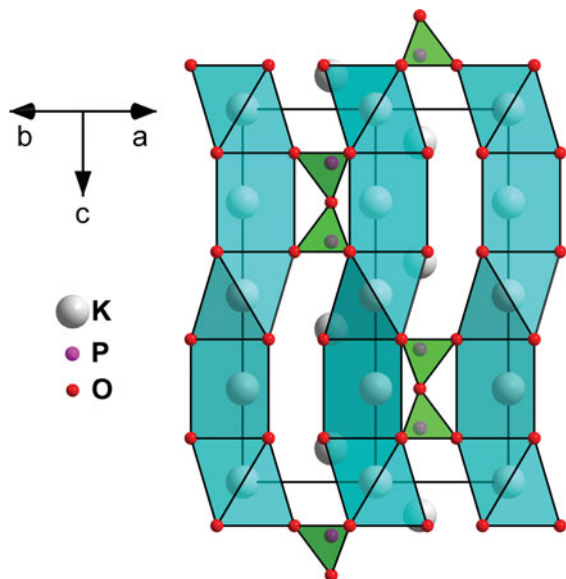
Figure 6. View of the structure of γ-$K_4P_2O_7$ at 300 °C showing the columns of potassium atoms K2 and K3 alternating $K3O_6$ octahedra and $K2O_6$ TPs sharing faces along the *c*-axis.

Figure 7. $K1O_9$ polyhedra in γ-$K_4P_2O_7$ at 300 °C opposing their hexagonal faces.

displaced so as to share with either an edge or a corner, and a supplementary oxygen atom may contribute to potassium coordination on the other side of the pentagonal face. According to this description, the $K1O_7$ polyhedron coordination is 5 + 2, close to be a monocapped TP; $K2O_8$ has a 1
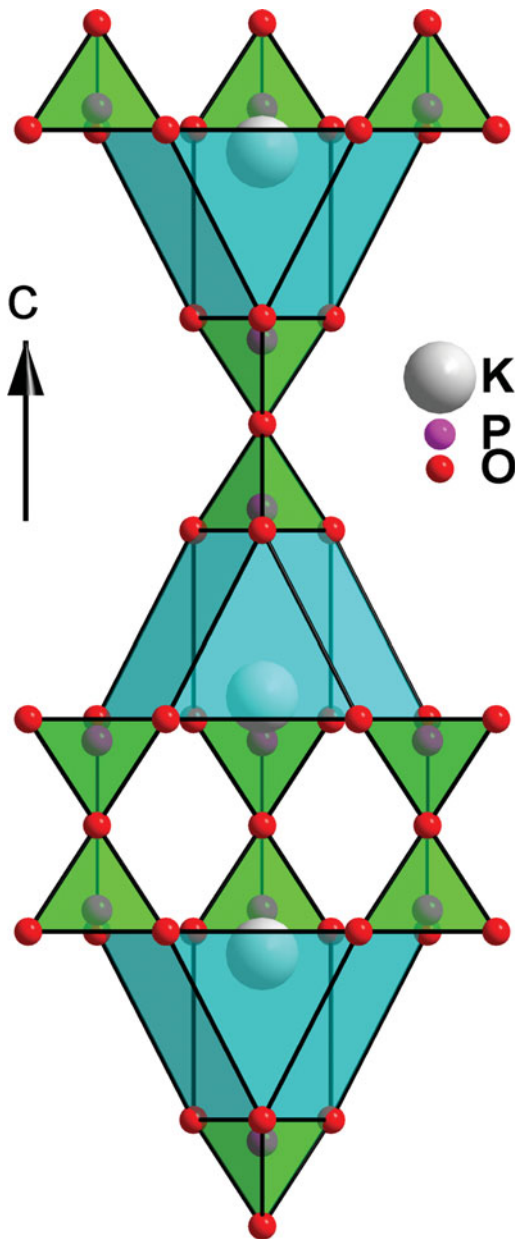
+ 5 + 2 coordination; $K5O_8$, $K7O_8$, and $K8O_8$ have lost one oxygen atom of the hexagonal plane but still share a face with a PO_4 tetrahedron, leading to the 5 + 3 coordination;
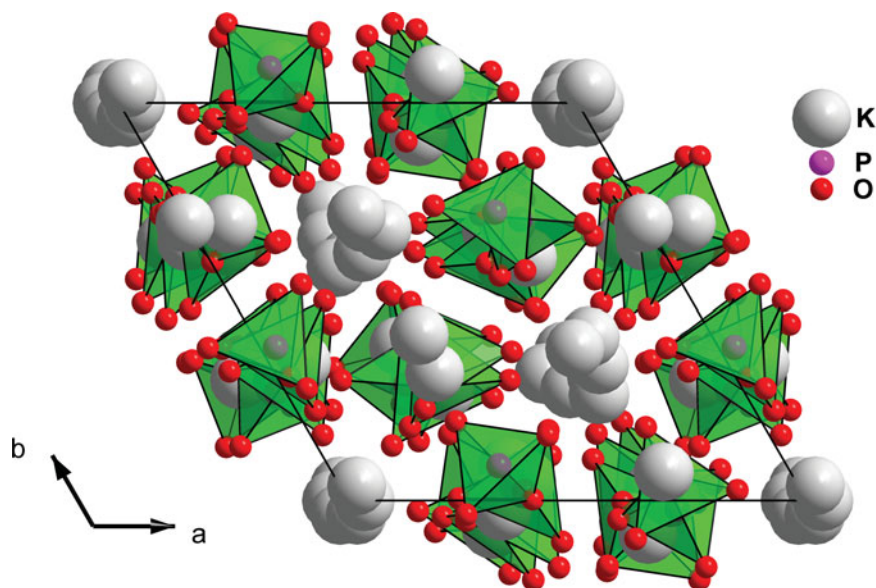
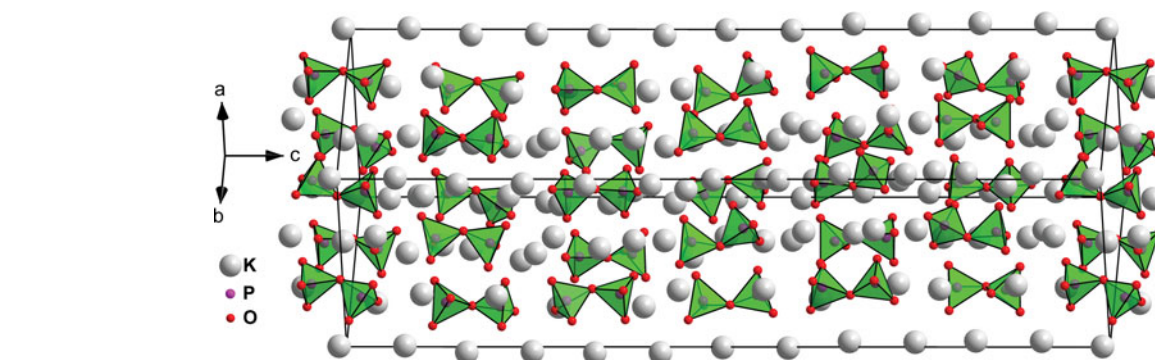Figure 8. Projection along the *c*-axis of the structure of δ-K$_4$P$_2$O$_7$.

Figure 9. Projection along the [110]-direction of the structure of δ-K$_4$P$_2$O$_7$.

K6O$_7$ can be described as a 1 + 5 + 1 pentagonal bipyramid. For those K3, K9, and K10 atoms of the δ-form, forming the K2O$_6$ TP in the γ-form, K3O$_8$ is a highly distorted bicapped TP; K9O$_9$ looks like a very distorted tricapped TP, the main distortion coming from face sharing with a PO$_4$ tetrahedron; K10O$_6$ is a TP. For those K4, K11, and K12 atoms of the δ-form, forming the K3O$_6$ octahedra in the γ-form, K4O$_6$ and K12O$_6$ are both octahedra and K11O$_7$ is a monocapped TP. Two of the three different [P$_2$O$_7$]$^{4-}$ groups are staggered (average torsion angles O–P1···4–O = 60° and O–P2···P3–O = 67°), the third is eclipsed (O–P5···P6–O = 11°). This complex ordering at room temperature is probably not free from stacking faults along the *c*-axis, as suggested by the anisotropic line broadening and the fact that the 00*l* lines are the broadest. This broadening, intrinsic to the sample, considerably decreases the resolution and explains the difficulties in refining all coordinates without distance restraints in the [P$_2$O$_7$]$^{4-}$ groups, despite the use of instrumental high-resolution synchrotron powder data. Finally, the bond valence calculations (Table VI) look better than for the γ-form, though K10, in a TP, presents a large bond valence (1.45 instead of 1). The very similar bond valence values for the six P atoms (4.82 ± 0.02 instead of five) is the consequence of the distance restraint on the PO$_4$ tetrahedra.

V. CONCLUSION

The γ-form of K$_4$P$_2$O$_7$ is shown to be related to the orthorhombic form of Na$_4$P$_2$O$_7$, whereas the room temperature form δ-K$_4$P$_2$O$_7$ is derived from the γ-form by considerable atom shifts leading to a hexagonal supercell nine times larger in volume. The existence of the β-K$_4$P$_2$O$_7$ form is not confirmed at the temperature previously announced. However, since the maximum temperature attained in this study is 700 °C, less than the expected α/β transition, and given the large number of papers where δ- and γ-K$_4$P$_2$O$_7$ are cited since 1978, their Greek letter numbering was not changed. More work is needed in order to characterize the additional events (220–250 °C) observed in the fast-heating-rate neutron data.

SUPPLEMENTARY MATERIALS AND METHODS

The Supplementary material referred to in this article can be found online at journals.cambridge.org/pdj.

ACKNOWLEDGEMENT

Brese, N. E. and O'Keefe, M. (**1991**). "Bond-valence parameters for solids," Acta Crystallogr. **B47**, 192–197.

de Wolf, P. M. (**1968**). "A simplified criterion for the reliability of a powder pattern indexing," J. Appl. Crystallogr. **1**, 108–113.

Dowty, E. (**2006**). CRYSCON, version 1.2.1, Shape Software, Kingsport, USA.

Dumas, Y. and Galigné, J. L. (**1974**). "Structure cristalline du pyrophosphate tétrapotassique trihydraté, $K_4P_2O_7 \cdot 3H_2O$," Acta Crystallogr. **B30**, 390–395.

Durif, A. (**1995**). *Crystal Chemistry of Condensed Phosphates* (Plenum Press, New York) p. 17.

Fitch, A. N. (**2004**). "The high resolution powder diffraction beam line at ESRF," J. Res. Natl. Inst. Stand. Technol. **109**, 133–142.

Gražulis, S., Chateigner, D., Downs, R. T., Yokochi, A. F. T., Quirós, M., Lutterotti, L., Manakova, E., Butkus, J., Moeck, P. and Le Bail, A. (**2009**). "Crystallography Open Database – an open-access collection of crystal structures," J. Appl. Crystallogr. **42**, 726–729.

Le Bail, A. (**2001**). "ESPOIR: a program for solving structures by Monte Carlo from powder diffraction data," Mater. Sci. Forum **378–381**, 65–70.

Le Bail, A. (**2004**). "Monte Carlo indexing with McMaille," Powder Diffr. **19**, 249–254.

Le Bail, A. (**2005**). "Whole powder pattern decomposition methods and applications – a retrospection," Powder Diffr. **20**, 316–326.

Le Bail, A. (**2008**). "Structure solution," in *Principles and Applications of Powder Diffraction*, edited by A. Clearfield, J. Reibenspies and N. Bhuvanesh (Wiley, New York), pp. 261–309.

Le Bail, A, Cranswick, L. M. D., Adil, K., Altomare, A., Avdeev, M., Cerny, R., Cuocci, C., Giacovazzo, C., Halasz, I., Lapidus, S. H., Louwen, J. N., Moliterni, A., Palatinus, L., Rizzi, R., Schilder, E. C., Stephens, P. W., Stone, K. H., and van Mechelen, J. (**2009**). "Third structure determination by powder diffractometry round robin (SDPDRR-3)," Powder Diffr. **24**, 254–262.

Leung, K. Y. and Calvo, C. (**1972**). "The structure of $Na_4P_2O_7$ at 22 °C," Can J. Chem. **50**, 2519–2526.

Morey, G. W., Boyd, Jr F. R., England, J. L. and Chen, W. T. (**1955**). "The system $NaPO_3$–$Na_4P_2O_7$–$K_4P_2O_7$–KPO_3," J. Am. Chem. Soc. **77**, 5003–5011.

Napper, J. D., Layland, R. C., Smith, M. D. and zur Loye, H.-C. (**2004**). "Crystal growth and structure determination of the new silicate $K_3ScSi_2O_7$," J. Chem. Crystallogr. **34**, 347–351.

Rietveld, H. M. (**1969**). "A profile refinement method for nuclear and magnetic structures," J. Appl. Crystallogr. **2**, 65–71.

Rodriguez-Carvajal, J. (**1993**). "Recent advances in magnetic-structure determination by neutron powder diffraction," Physica B, **192**, 55–69.

Sandström, M. (**2006**). "Structural and solid state EMF studies of phases in the CaO–K_2O–P_2O_5 system with relevance for biomass combustion," PhD Thesis, Umeå University, Sweden.

Sandström, M., Fischer, A. and Boström, D. (**2003**). "$CaK_2P_2O_7$," Acta Crystallogr. **E59**, i139–i141.

Shekhtman, G. Sh., Smirnov, N. B. and Burmakin, E. I. (**2000**). "Electroconductivity of solid solutions in the $K_4P_2O_7$-$Rb_4P_2O_7$ system," Russ. J. Electrochem. **36**, 435–437.

Sheldrick, G. (**2008**). "A short history of SHELX," Acta Crystallogr. **A64**, 112–122.

Smith, G. S. and Snyder, R. L. (**1979**). "FN: a criterion for rating powder diffraction patterns and evaluating the reliability of powder-pattern indexing," J. Appl. Crystallogr. **12**, 60–65.

Szczygieł, I., Znamierowska, T. and Mizer, D. (**2010**). "Phase equilibria in the oxide system Nd_2O_3–K_2O–P_2O_5," Solid State Sci. **12**, 1205–1210.

Vidican, I., Smith, M. D. and zur Loye, H. -C. (**2003**). "Crystal growth, structure determination, and optical properties of new potassium-rare-earth silicates $K_3RESi_2O_7$ (RE = Gd, Tb, Dy, Ho, Er, Tm, Yb, Lu)," J. Solid State Chem. **179**, 203–210.

Znamierowska, T. (**1978**). "Phase equilibria in the system CaO–K_2O–P_2O_5. Part III. The partial system $CaK_2P_2O_7$–$K_4P_2O_7$–KPO_3," Pol. J. Chem. **52**, 1889–1895.